Structural Engineering and Mechanics, Vol. 27, No. 4 (2007) 501-521 501
DOI: http://dx.doi.org/10.12989/sem.2007.27.4.501

Strength and deflection prediction of double-curvature reinforced concrete squat walls

Ika Bali†

Department of Civil Engineering, Universitas Kristen Indonesia, Jalan Mayjen Sutoyo, Cawang, 13630, Indonesia

Shyh-Jiann Hwang‡

Department of Civil Engineering, National Taiwan University, Taipei, 10617, Taiwan

(Received October 16, 2006, Accepted April 14, 2007)

Abstract. This study presents a model to better understand the shear behavior of reinforced concrete walls subjected to lateral load. The scope of the study is limited to squat walls with height to length ratios not exceeding two, deformed in a double-curvature shape. This study is based on limited knowledge of the shear behavior of low-rise shear walls subjected to double-curvature bending. In this study, the wall ultimate strength is defined as the smaller of flexural and shear strengths. The flexural strength is calculated using a strength-of-material analysis, and the shear strength is predicted according to the softened strut-and-tie model. The corresponding lateral deflection of the walls is estimated by superposition of its flexibility sources of bending, shear and slip. The calculated results of the proposed procedure correlate reasonably well with previously reported experimental results.

Keywords: reinforced concrete; double-curvature; squat wall; shear wall; strength; deflection; strut; tie.

1. Introduction

The seismic-resistant structural systems of reinforced concrete structural buildings generally use either moment resisting space frames, shear walls or a combination of both. However, shear wall systems exhibit better performance than space frame systems do (Fintel 1991).

Shear walls, which are used in lateral force resisting systems, can exhibit either ductile or non-ductile behavior. The ductile shear walls develop a flexural-ductile mode of failure if a severe earthquake occurs, while the non-ductile shear walls exhibit a shear mode of failure.

The non-ductile shear walls are appropriate for low-rise buildings due to their efficiency and economy. Shear walls are thus extensively used in low-rise buildings in the form of reinforced concrete squat walls, which have height to length ratios not exceeding 2. The predominant action of such walls is shear, and the flexural yielding is limited due to the shear failure mode of the walls.

† Ph.D., Lecturer, Corresponding author, E-mail: ikabali@yahoo.com
‡ Professor, E-mail: sjhwang@ntu.edu.tw

Shear behavior of reinforced concrete squat walls subjected to single-curvature bending can be reasonably predicted using the softened strut-and-tie (SST) model (Hwang *et al.* 2001, Yu and Hwang 2005, Tu *et al.* 2006). The model proposed in this paper employed this concept.

This study considers the potential double-curvature deformation of squat walls in real structures. For structures designed with seismic resistance, the top of wall is always connected to the strong diaphragm. Due to this connection, rotation atop the wall is constrained. This condition is more likely to cause a double-curvature behavior of wall.

This study presents a model for predicting the ultimate strength and corresponding deflection of double-curvature reinforced concrete squat walls. The ultimate strength is defined as the smaller of flexural and shear strengths. The flexural strength is calculated using a strength-of-material analysis, and the shear strength is predicted using the SST model. Estimation of the corresponding lateral deflection is attained using superposition of its flexibility sources of bending, shear and slip (Sozen *et al.* 1992).

2. Double-curvature wall

Walls in real condition of low-rise buildings may deform in a double-curvature shape if the top of wall is connected to the strong diaphragm. Hidalgo *et al.* (2002) and Lopes (1991) simulated a double-curvature bending by testing wall specimens in experimental conditions designed to prevent the rotation of both the top and bottom ends of the specimen. Based on this condition, analytical modeling of the double-curvature wall is described as follows.

Single and double-curvature walls are different in shear behaviors, so that the shear element and its modeling are also different. The major difference in modeling the single and double-curvature walls that is proposed in this study is to define shear element of the walls. The shear element of a wall has height ℓ_v and length ℓ_h (Fig. 1).

In the case of single-curvature walls (Hwang *et al.* 2001, Yu and Hwang 2005, and Tu *et al.* 2006), it is proposed to consider $\ell_v = H$, where H is the distance measured from the center of top

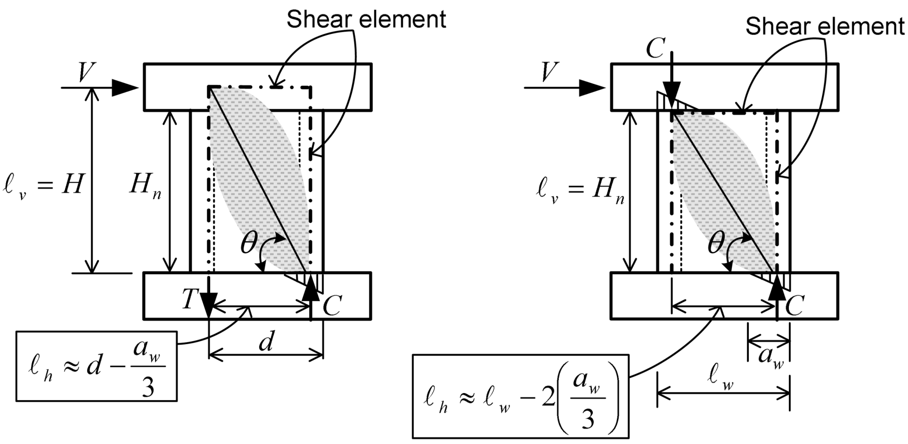

(a) Single-curvature wall (b) Double-curvature wall

Fig. 1 Shear element of walls

beam to the wall base, and ℓ_h is equal to the horizontal distance from the point of tension force to the point of the resultant of the compression force of the wall (Fig. 1(a)).

For double-curvature wall specimens, the top beam of walls is large and set up as a fixed support; therefore, it could be assumed as a rigid beam. In this case, instead of the center of top beam, which is usually used in single-curvature walls, shear friction between the top beam and the wall panel could be adopted as the ceiling of the shear element of double-curvature walls. Hence, the height of shear element ℓ_v for a double-curvature wall is assumed to be the clear height of the wall panel, H_n. The value of ℓ_h for double-curvature walls can be estimated as the horizontal distance measured between the points of resultant compressive force at the top and bottom wall (Fig. 1(b)) due to the assumption that the concentrated flow of stresses along the diagonal strut will end at the point of compressive force.

Considering the above assumptions for the shear element, the inclination angle of the diagonal strut for double-curvature squat walls can be defined as

$$\theta = \tan^{-1}\left(\frac{\ell_v}{\ell_h}\right) \tag{1}$$

where $\ell_v = H_n$, $\ell_h \approx \ell_w - 2(a_w/3)$; ℓ_w denotes the length of the entire wall in direction of shear force, and a_w is the distance from the extreme compression fiber to the neutral axis when the flexural moment reaches the yielding moment.

For the case of single-curvature walls (Hwang *et al.* 2001, Yu and Hwang 2005, Tu *et al.* 2006), the angle of inclination of the diagonal strut with respect to the horizontal axis h is defined as $\theta = \tan^{-1}(H/\ell_h)$, where $\ell_h \approx d - (a_w/3)$, and d is the distance from the extreme compression fiber to the center of the resultant force of all reinforcements in tension.

3. Prediction of strength

This study defines the ultimate strength of reinforced concrete squat walls as the smaller of flexural and shear strengths as given by

$$V_u = \text{smaller of } (V_f,\ V_s) \tag{2}$$

where V_u is the ultimate strength of the wall, V_f denotes the flexural strength of the walls, which is the maximum shear force associated to the flexural failure mode regardless of the value of shear, and V_s denotes the shear strength of the walls, which is the maximum shear force associated to shear failure mode regardless of the value of bending moment.

The flexural strength of the wall caused by double curvature bending can be calculated as

$$V_f = \frac{M_t + M_b}{H_n} \tag{3}$$

where M_t and M_b is the flexural moment at the top and bottom of walls, respectively.

Based on the fully cracked assumption of the wall shear element, the shear strength V_s can be predicted using the simplified version of the softened strut-and-tie model (Hwang and Lee 2002). Fig. 2(a) shows the strut-and-tie modeling for the cracked double-curvature RC squat wall. The formation of the softened strut-and-tie action can be explained as follows.

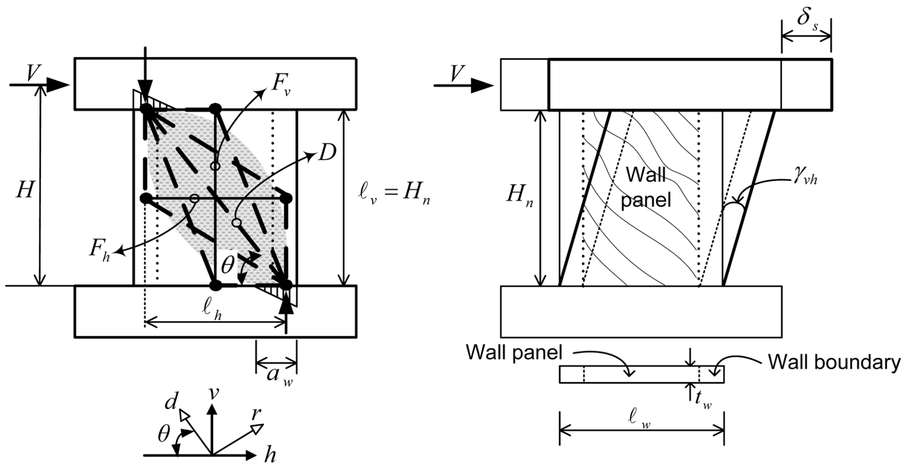

(a) Strut-and-tie modeling for cracked wall (b) Shear deflection of wall

Fig. 2 Strut-and-tie modeling for double-curvature wall

After the development of the cracking pattern in the wall, the steel bars are subjected to tension, and the concrete acts as a compressive strut, thus forming a strut-and-tie action. Shear failure of the wall occurs when the concentrated flow of stresses along the diagonal strut surpasses the compressive capacity of the cracked reinforced concrete in the panel. The influence of the softened effect on concrete is thus considered for the concrete strength (Vecchio and Collins 1993, Zhang and Hsu 1998). This model is called the softened strut-and-tie model, since it considers the softening effect, which weakens the concrete strength. The main steps of the SST model for predicting the shear strength are described as below.

The shear strength of reinforced concrete squat walls failing in diagonal compressions can be estimated as (Hwang and Lee 2002)

$$V_s = K\zeta f_c' A_{str} \cos\theta \tag{4}$$

where K is the strut-and-tie index and $K = (K_h + K_v - 1)$, A_{str} is the effective area of the diagonal strut, and the softening coefficient ζ is approximated as (Hwang and Lee 2002)

$$\zeta \approx \frac{3.35}{\sqrt{f_c'}} \le 0.52 \tag{5}$$

where f_c' is the compressive strength of a standard concrete cylinder in units of MPa.

The horizontal tie index K_h is expressed as

$$K_h = 1 + \frac{(\overline{K}_h - 1)A_{th} f_{yh}}{\overline{F}_h} \le \overline{K}_h \tag{6}$$

where A_{th} is the area of the horizontal tie, f_{yh} represents the yield strength of horizontal reinforcement, and $\overline{K}_h$ is the horizontal tie index with sufficient horizontal reinforcement, and can be estimated as

$$\overline{K}_h \approx \frac{1}{1 - 0.2(\gamma_h + \gamma_h^2)} \tag{7}$$

where γ_h is the fraction of diagonal compression carried by the horizontal tie in the absence of the vertical tie, and is defined as (CEB-FIP Model Code 1990, 1993)

$$\gamma_h = \frac{2\tan\theta - 1}{3} \quad \text{for} \quad 0 \le \gamma_h \le 1 \tag{8}$$

$\overline{F}_h$ is the balanced amount of the horizontal tie force, and is given by

$$\overline{F}_h = \gamma_h \times (\overline{K}_h \zeta f_c' A_{str}) \times \cos\theta \tag{9}$$

The equations for the vertical tie index K_v are the same as Eq. (6) to Eq. (9), except that each subscript h is replaced by v, and $\cos\theta$ and $\sin\theta$ are interchanged.

The effective area of the diagonal strut A_{str} is defined as

$$A_{str} = a_w \times t_w \tag{10}$$

where t_w is the width of the wall web, and a_w can be determined by sectional analysis for the stage when the extreme tensile steel reaches yielding.

4. Prediction of deflection

In this study, the ultimate lateral deflection of wall is estimated as the superposition of the flexibility sources of shear, flexure, and slip

$$\delta_u = \delta_s + \delta_f + \delta_{slip} \tag{11}$$

where δ_u is the ultimate lateral deflection of the wall along the axis of the horizontal load, and δ_s, δ_f and δ_{slip} are the wall deflections due to shear, flexure and slip, respectively.

The shear deflection of the wall (Fig. 2(b)) is estimated by assuming that the wall panel is subjected to uniform shear strain (Hsu 1993), and is expressed as (Tu *et al.* 2006)

$$\delta_s = \gamma_{vh} H_n \tag{12}$$

where γ_{vh} is the average shear strain in the wall panel. The estimation of γ_{vh} for the cracked reinforced concrete panel is based on the softened strut-and-tie model, and it is described below.

The average strains of a cracked wall panel as postulated by the SST model are assumed to meet the requirements of Mohr's compatibility (Tu *et al.* 2006). Under that assumption, the average shear strain in the v- and h-coordinate system γ_{vh} can be expressed as

$$\gamma_{vh} = 2(\varepsilon_r - \varepsilon_d)\sin\theta\cos\theta \tag{13}$$

where ε_r and ε_d are the average principal strains in the r- and d-directions, respectively (positive for tension) (Fig. 2(a)).

Since the sum of the normal strains in the perpendicular direction is a constant, this compatibility condition requires

$$\varepsilon_r = \varepsilon_h + \varepsilon_v - \varepsilon_d \tag{14}$$

where ε_h and ε_v are the average strains in the h- and v-directions, respectively (positive for tension). These strains can be obtained from the tension forces in the horizontal and vertical ties, and suggested not greater than the yielding strain. This limitation should be set to these strains to avoid the overestimation of the softening of the concrete (Vecchio and Collins 1993). So, ε_h and ε_v are defined as

$$\varepsilon_h = \frac{F_h}{A_{th}E_s} \le \varepsilon_y \tag{15}$$

$$\varepsilon_v = \frac{F_v}{A_{tv}E_s} \le \varepsilon_y \tag{16}$$

where F_h and F_v are the tension forces of the horizontal and vertical ties, respectively, A_{tv} is the area of the vertical tie, E_s is the modulus of elasticity of steel bar, and ε_y is the yield strain of steel.

The tension tie forces at ultimate load can be determined according to their relative stiffness ratios (Hwang and Lee 2002).

$$F_h = R_h V_u \tag{17}$$

$$F_v = R_v V_u \tan\theta \tag{18}$$

where R_h and R_v are the wall shear ratios resisted by the horizontal and vertical mechanisms, respectively, obtained as

$$R_h = \frac{\gamma_h(1-\gamma_v)}{1-\gamma_h\gamma_v} \tag{19}$$

$$R_v = \frac{\gamma_v(1-\gamma_h)}{1-\gamma_h\gamma_v} \tag{20}$$

where γ_v is the fraction of diagonal compression carried by the vertical tie in the absence of the horizontal tie.

The values of ε_d should be determined from the softened laws of cracked concrete. According to Zhang and Hsu (1998), the maximum strength of the softened concrete $\zeta f_c'$ occurs at the strain of $\zeta\varepsilon_o$. Thus, the value of ε_d associated with the ultimate deflection δ_u is approximated as

$$-\varepsilon_d = \zeta\varepsilon_0 \tag{21}$$

where ε_0 is the concrete cylinder strain corresponding to the cylinder strength f_c'. The value of ε_0 can be defined approximately as (Foster and Gilbert 1996)

$$\varepsilon_0 = 0.002 + 0.001\left(\frac{f_c' - 20}{80}\right) \quad \text{for} \quad 20 \le f_c' \le 100\,\text{MPa} \tag{22}$$

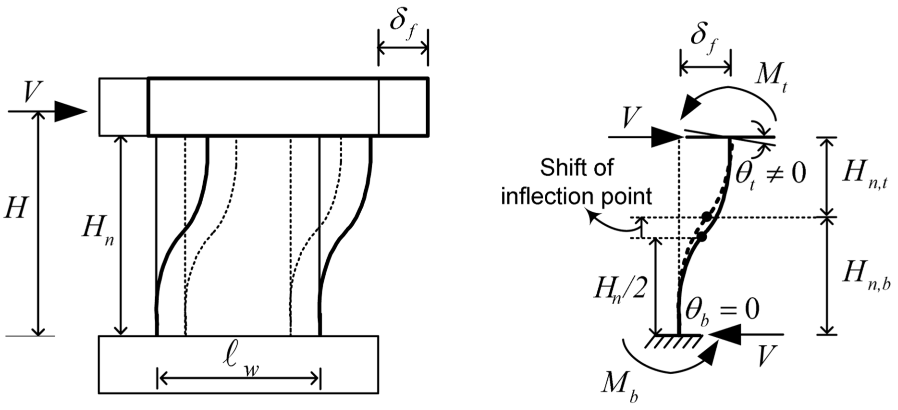

(a) Double-curvature bending

(b) Displacement and rotation at the top of wall

Fig. 3 Flexural deflection of wall

In this study, it was considered that $\varepsilon_0 = 0.002$ for $f_c' < 20$ MPa.

Since the expected failure mode of the walls is mainly shear, this study assumes that the flexural and slip deflections are in elastic range. The flexural deflection of the wall, resulting from double curvature bending as shown in Fig. 3(a), can be determined as follows.

Considering the wall with fixed end support at the bottom, and subjected to lateral displacement and rotation at the top of wall (Fig. 3(b)), the flexural lateral deflection of the wall in terms of M_t and M_b can be estimated as,

$$\delta_f = \frac{H_n^2}{6E_cI_e}(2M_b - M_t) \tag{23}$$

where E_c is the modulus of elasticity of concrete (=$4700\sqrt{f_c'}$, where f_c' in MPa), I_e is the effective moment of inertia of the wall section, and assumed as $I_e = 0.35I_g$ (ACI 318-05), and I_g is the moment of inertia of the gross concrete section.

From the relationship indicated in Fig. 3(b), flexural moment at the top and bottom walls, M_t and M_b at ultimate load can be expressed by the equations as follows

$$M_t = V_uH_{n,t} \tag{24}$$

$$M_b = V_uH_{n,b} \tag{25}$$

where $H_{n,t}$ is the distance from the inflection point to the bottom of top beam, and can be calculated as $H_{n,t} = [M_t/(M_t + M_b)]H_n$, and $H_{n,b}$ is the distance from the inflection point to the wall base, and can be expressed as $H_{n,b} = [M_b/(M_t + M_b)]H_n$.

Substituting Eqs. (24) and (25) into Eq. (23), the flexural lateral deflection can be expressed in terms of $H_{n,t}$ and $H_{n,b}$, that is

$$\delta_f = \frac{V_uH_n^2}{6E_cI_e}(2H_{n,b} - H_{n,t}) \tag{26}$$

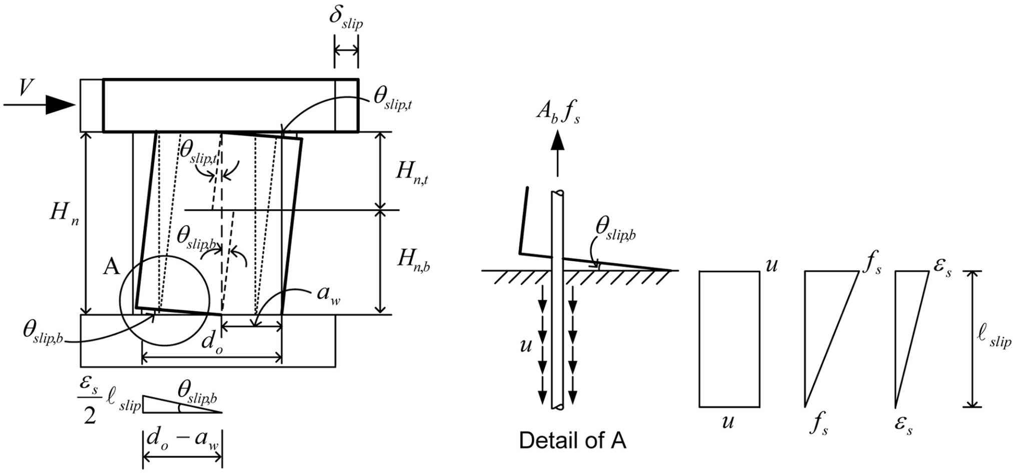

(a) Slip due to double-curvature bending (b) Assumed bar strain and stress distributions

Fig. 4 Slip deflection of wall

Eq. (26) corresponds to the flexural lateral deflection caused by shifting of the bending inflection point in double-curvature walls.

Vecchio (1998) reported that bond and anchorage slip at wall base is possibly a significant factor in total deflection contribution of shear walls, particularly for the walls under cyclic load. Slip deflection of the wall, resulting from double-curvature bending (Fig. 4), is defined as the sum of the slip deflections of the top and bottom wall (Sezen 2002), and can be expressed as

$$\delta_{slip} = \theta_{slip,\,t}H_{n,\,t} + \theta_{slip,\,b}H_{n,\,b} \tag{27}$$

where $\theta_{slip,\,t}$ and $\theta_{slip,\,b}$ are the slip rotation at the top and bottom of the walls, respectively.

The slip rotation of the wall when the stresses of the steel bars are within the elastic range $f_s \le f_y$ can be estimated as

$$\theta_{slip} = \frac{d_b f_s^2}{8uE_s(d_o - a_w)} \tag{28}$$

where d_b is the diameter of the outmost tension steel bar, f_s is the stress of the outmost steel bar when V_u occurs, u is average bond stress, assumed herein as $u = \sqrt{f_c'}$ (Sezen 2002) (f_c' in units of MPa), and d_o represents the distance from extreme compression fiber to the center of the outmost tension steel bar.

Fig. 5 summarizes proposed procedure to estimate the ultimate strength and the corresponding deflection of double-curvature walls.

5. Experimental verification

A total of 19 test specimens of shear walls with a height-to-length ratio less than 2 available in the technical literature (Lopes 1991, Hidalgo *et al.* 2002) were used to verify the prediction of the model. The specimens were selected to satisfy the following conditions: (1) the test specimen must be a wall with double-curvature bending; (2) the test specimen must fail in the wall panel shear mode; (3) the test specimen must be a one-story isolated wall with a height-to-length ratio less than 2; (4) the specimen must contain both horizontal and vertical reinforcement uniformly distributed through the wall panel.

The distance from the inflection point to the bottom of the top beam in the specimens of Lopes (1991) was $H_{n,t} = 0.42H$. The shift of bending inflection point in the specimens of Hidalgo *et al.* (2002) was very small, therefore $H_{n,t}$ can be taken as $0.5H_n$.

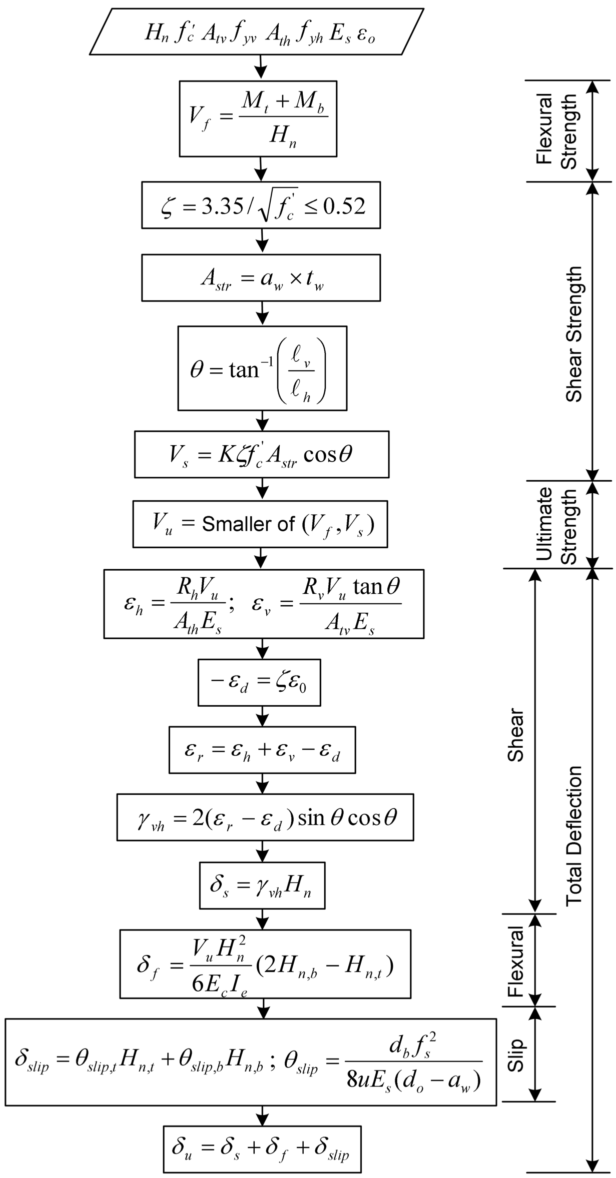

Fig. 5 Overview of the proposed procedure

The prediction of failure mode of the specimens is shear failure. This prediction agrees with the experimental failure mode of the specimens in this study.

5.1 Experimental verification for Lopes' specimens

The accuracy of the proposed model was verified in terms of the ratios of the measured to the calculated values. Table 1, Fig. 6 and Fig. 7 show ultimate strength and deflection predictions for the proposed model. For specimens SW11 to SW15 the average test-to-calculated strength ratio for the specimens was 1.20, and the coefficient of variation (COV) was 0.07 (Table 1 and Fig. 6). The average test-to-calculated deflection ratio for the specimens was 1.02, and the COV was 0.34 (Table 1 and Fig. 6). Fig. 7 shows that the calculated strength and corresponding deflection reasonably fit

Table 1 Experimental verification

No.	Specimen	$H_n \times \ell_w \times t_w$ cm	f_c' MPa	ρ_v %	f_{yv} MPa	ρ_h %	f_{yh} MPa	$V_{u,test}$ kN	$\delta_{u,test}$ mm	$\frac{V_{u,test}}{V_{u,calc}}$	$\frac{\delta_{u,test}}{\delta_{u,calc}}$
					Lopes (1991)						
1	SW 11	85.5×45×4.5	40.1	0.41	414	0.92	414	93	4.7	1.21	1.09
2	SW 12	85.5×45×4.5	41.2	0.41	414	0.92	414	88	3.1	1.13	0.71
3	SW 13	85.5×45×4.5	47.8	0.41	414	0.92	414	105	7.0	1.30	1.64
4	SW 14	85.5×45×4.5	40.4	0.41	414	0.92	414	98	4.2	1.28	0.96
5	SW 15	85.5×45×4.5	41.3	0.41	414	0.62	414	85	3.2	1.09	0.70
									AVG	1.20	1.02
									COV	0.07	0.34
					Hidalgo *et al.* (2002)						
6	1	200×100×12	19.4	0.25	392	0.13	392	198	13.2	1.14	1.76
7	2	200×100×12	19.6	0.25	402	0.25	402	270	15.0	1.29	1.87
8	4	200×100×12	19.5	0.25	402	0.38	402	324	15.0	1.35	1.89
9	6	180×130×12	17.6	0.26	314	0.13	314	309	7.9	1.32	1.16
10	7	180×130×12	18.1	0.13	471	0.25	471	364	11.3	1.28	1.32
11	8	180×130×12	15.7	0.26	471	0.25	471	374	9.9	1.41	1.20
12	9	180×130×10	17.6	0.26	366	0.26	366	258	9.7	1.16	1.31
13	10	180×130×8	16.4	0.25	367	0.25	367	187	8.3	1.09	1.16
14	11	140×140×10	16.3	0.26	362	0.13	362	235	4.9	0.99	0.67
15	12	140×140×10	17.0	0.13	366	0.26	366	304	7.0	1.22	0.83
16	13	140×140×10	18.1	0.26	370	0.26	370	289	4.9	1.08	0.64
17	14	120×170×8	17.1	0.25	366	0.13	366	255	3.0	0.96	0.42
18	15	120×170×8	19.0	0.13	366	0.25	366	368	5.0	1.40	0.84
19	16	120×170×8	18.8	0.25	366	0.25	366	362	4.4	1.26	0.71
									AVG	1.21	1.13
									COV	0.11	0.40
									Total AVG	**1.21**	**1.10**
									Total COV	**0.10**	**0.39**

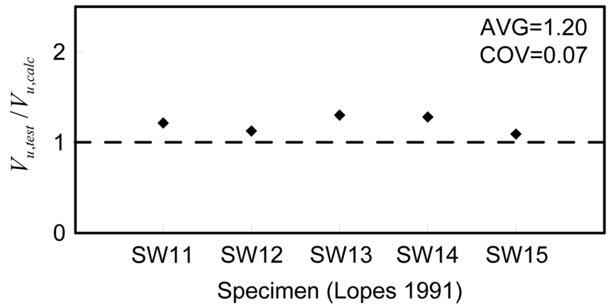

(a) Verification of ultimate strength

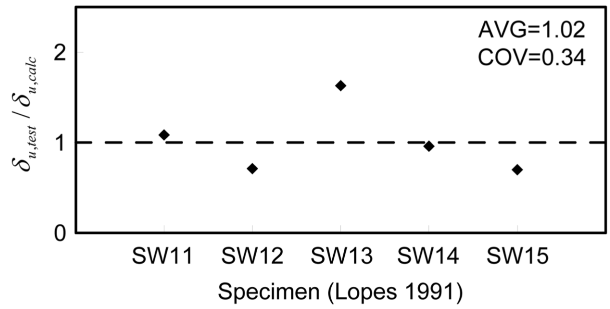

(b) Verification of deflection

Fig. 6 Predicted versus experimental results for Lopes' specimens

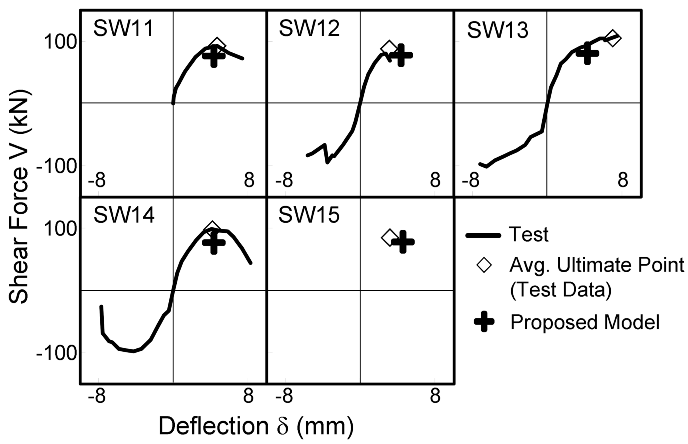

Fig. 7 Load-deflection curves for Lopes' specimens

the measured load-deflection curve. These results indicate that the proposed method reasonably matches the measured results.

Other measured quantities, such as the horizontal and vertical strains of the shear reinforcement are also compared. The horizontal strain of specimen SW13 and vertical strain of specimen SW 12 were selected for verification, since the complete data set was available. Fig. 8 shows the

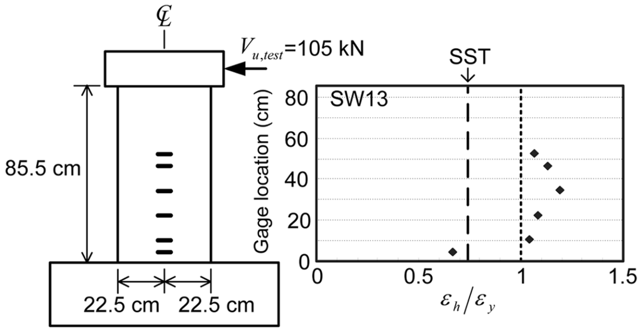

(a) Horizontal strains of SW 13 at V_u (Lopes 1991)

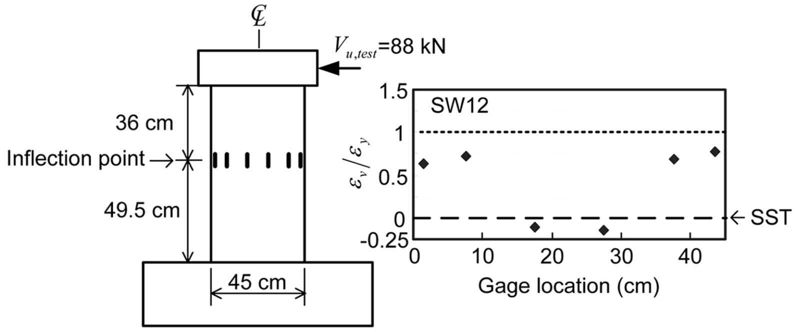

(b) Vertical strains of SW 12 at V_u (Lopes 1991)

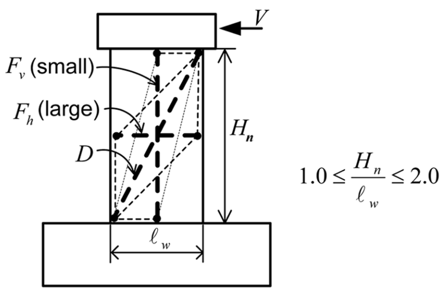

(c) Shear transfer mechanism

Fig. 8 Experimental verification of vertical and horizontal strains

comparison between the calculated average strains and measured strains of reinforcement. The calculated average strains were obtained from the estimated tension forces in the horizontal and vertical ties of entire walls.

For a height-to-length ratio of H_n/ℓ_w between 1 and 2, the SST model indicates that the horizontal shear reinforcement will be more effective to transfer the shear force compared with the vertical shear reinforcement (Fig. 8(c)). Since the height-to-length ratio of the specimens SW 13 and SW 12 is $H_n/\ell_w = 1.9$, the shear strength is mainly transferred by the horizontal shear reinforcement ($R_h = 1$ and $R_v = 0$). The dominant transfer of shear strength in horizontal shear reinforcement is verified by the very large measured strain of the horizontal shear reinforcement around the mid-height of wall, as shown in Fig. 8(a). By contrast, the shear force transfer by vertical shear reinforcement is extremely small, as shown by the negative value of the measured strain of vertical shear reinforcement around the vertical center line (Fig. 8(b)). These results show that the SST model correlates reasonably well with the force transfer mechanism of test specimens. In terms of strain estimations, the average horizontal strains of SST model are considerable lower than the measured horizontal strains (Fig. 8(a)). For the vertical strains, SST model has reasonable prediction in the middle and large deviation in both sides (Fig. 8(b)).

5.2 Experimental verification for Hidalgo et al.'s specimens

Table 1, Fig. 9 and Fig. 10 show the prediction of ultimate strength and corresponding deflection for the specimens 1 to 16. For those specimens, the average test-to-calculated strength ratio was 1.21, and the COV was 0.11. The deflection verification indicates that the average test-to-calculated deflection ratio for the specimens was 1.13, and the COV was 0.40. The mean value of deflection ratio is reasonably good however the value of COV is considerably large. Fig. 10 shows that the predicted ultimate strength and corresponding displacement reasonably fit the measured ones.

In Fig. 11, the effect of the horizontal shear reinforcement on shear strength was examined by comparing specimens 11 and 13, 6 and 8, and specimens 1 and 4. Those specimens were selected

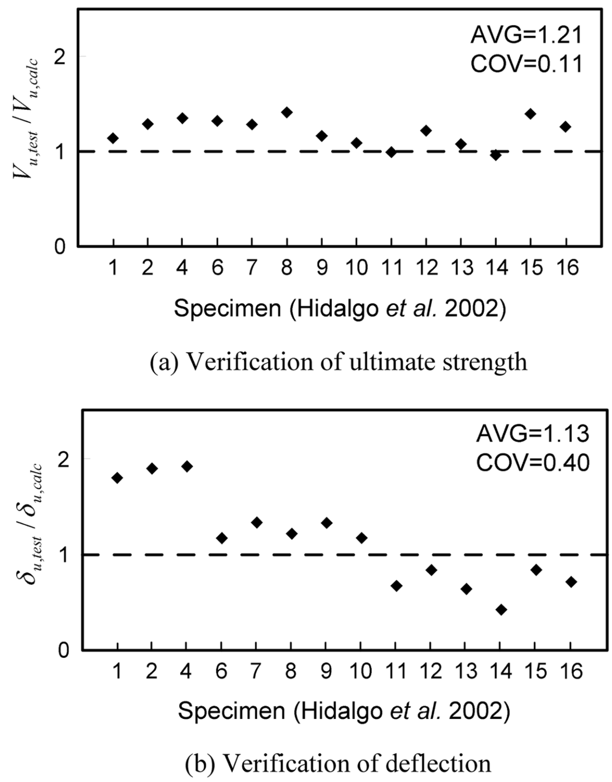

Fig. 9 Predicted versus experimental results for Hidalgo *et al.*'s specimens

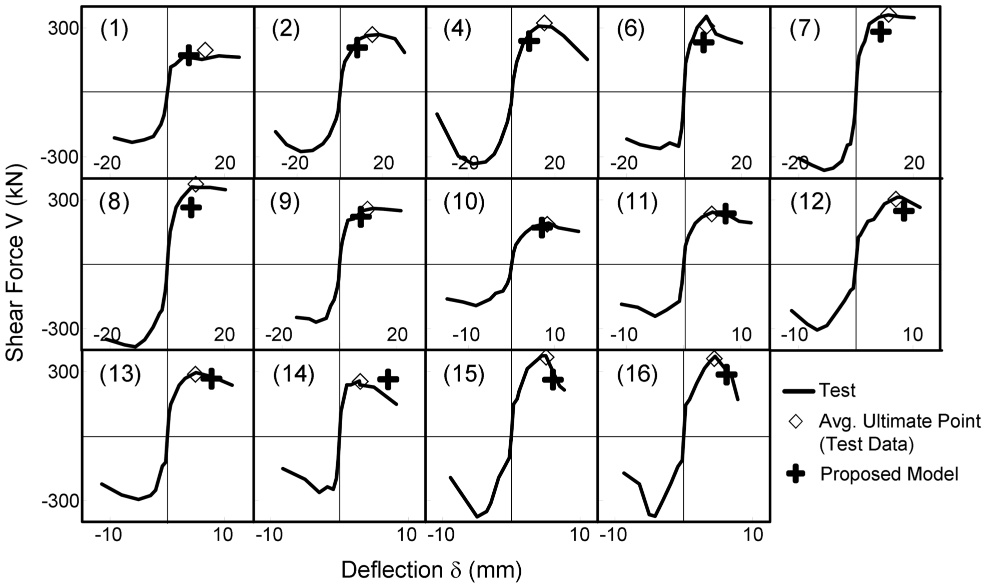

Fig. 10 Load-deflection curves for Hidalgo *et al.*'s specimens

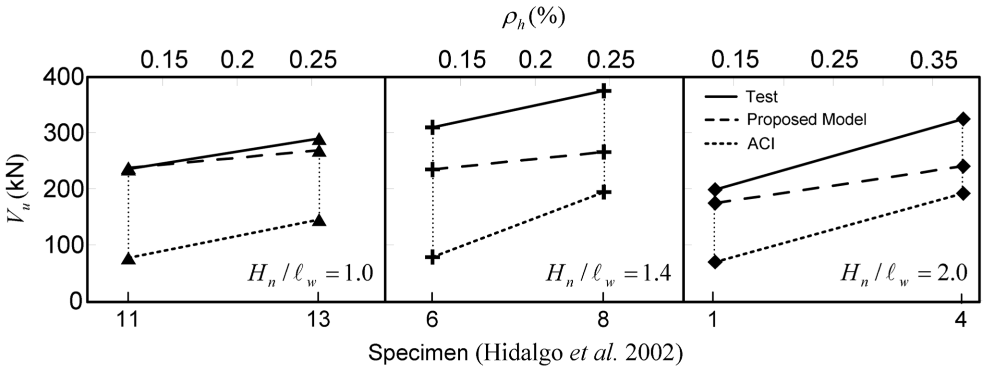

Fig. 11 Effect of horizontal reinforcement on shear strength

because they had similar characteristics, but different horizontal shear reinforcement ratios. Fig. 11 indicates that the shear strength increases with the increment in horizontal shear reinforcement ratio (ρ_h) for specimens with $1 \le H_n/\ell_w \le 2$.

Fig. 11 also shows the comparison among proposed model, test data, and ACI results. In this case, the ACI results are attained using the ACI equation (ACI 318-05) as follows

$$V_u = \left(\frac{1}{12}\alpha_c\sqrt{f_c'} + \rho_h f_{yh}\right)\ell_w t_w \le \frac{5}{6}\sqrt{f_c'}\,\ell_w t_w\,(\text{in MPa}) \tag{29}$$

where α_c is an coefficient which varies between 1/6 and 1/4 according to its height-to-width ratio (ACI 318-05).

As shown in Fig. 11, the ACI's prediction correlates well with the tendency of the measured shear

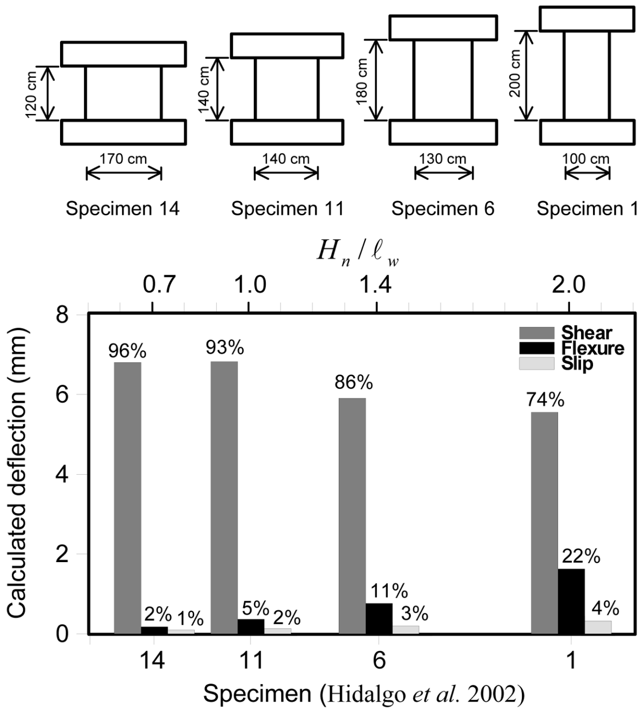

Fig. 12 Contribution of flexibility sources

strengths to increase with ρ_h, but the actual values of shear strength are very different from the experiment ones. In terms of the value of shear strengths, the proposed prediction is more accurate than the ACI's prediction.

The contribution of each source of flexibility to the total deflection of the walls was also studied. Fig. 12 shows the contributions of flexibility sources for specimens 14, 11, 6 and 1. According to Fig. 12, the shear deflection dominates (average of 87%) the total deflection contribution of walls with a height-to-length ratio H_n/ℓ_w in the range of 0.7 to 2.0. An increase in the H_n/ℓ_w ratio increases the contributions of flexural and slip deflection, and decreases the contribution of shear deflection. Fig. 12 also shows that specimen 1 with H_n/ℓ_w = 2.0 has the contribution of calculated flexural deflection up to 22% (calculated δ_f = 1.62 mm) of the total deflection. By contrast, the specimen 14 with H_n/ℓ_w = 0.7 has the contribution only 2% (calculated δ_f = 0.17 mm). The ratio of these calculated flexural deflections is about nine times.

5.3 Case study of single curvature versus double curvature

Specimen SW 11 (Lopes 1991) was selected for the case study of comparison of single and double-curvature walls. Ultimate strength and corresponding deflection of specimen SW11 were calculated using the single and double-curvature approaches. SST model is used for the predictions of shear strength and shear deflection. A comparison of these two approaches is presented. Fig. 13 compares the single and double curvature approaches for specimen SW11, which had a large H_n/ℓ_w ratio of 1.9. As indicated in Fig. 13(a), the single-curvature wall had a slender shear element, while

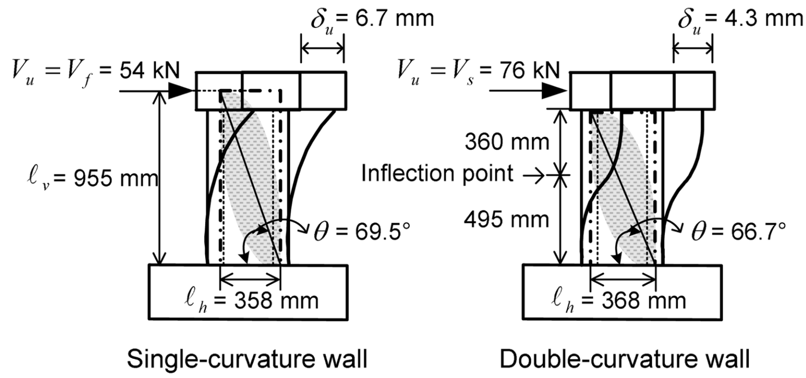

(a) Shear elements and predictions of specimen SW11 (Lopes 1991)

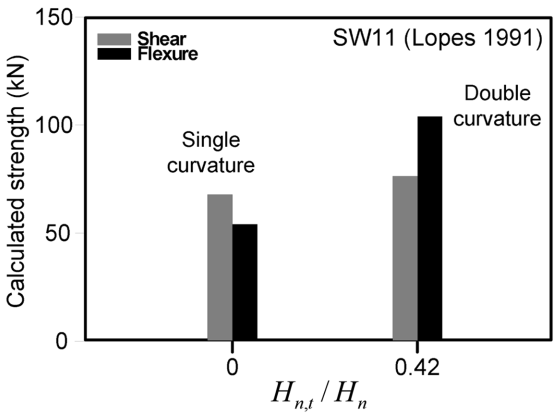

(b) Comparison of calculated strength

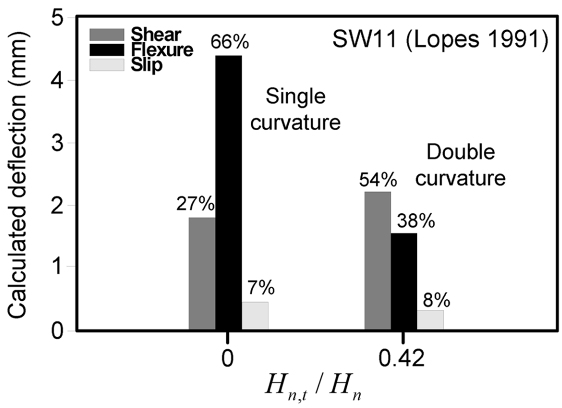

(c) Comparison of calculated deflection

Fig 13 Case study of single-curvature versus double-curvature

the double-curvature wall had a slight stocky shear element. Consequently, the inclination angle of the diagonal strut for the double-curvature wall, θ = 66.7°, was smaller than that of the single-curvature wall, θ = 69.5°. Since the calculated shear strength is proportional to the value of cosθ, therefore, the calculated shear strength of double-curvature wall was greater than the calculated shear strength of the single-curvature wall, as shown in Fig. 13(b). The difference between the calculated shear strengths of the single and double-curvature walls was around 13%. Due to the curvature bending, the calculated flexural strength of the double-curvature wall was 93% higher than that of the single-curvature wall. In this case study, the failure modes for the single and double-curvature walls were flexural and shear failures, respectively.

In terms of the contribution of flexibility sources, Fig. 13(c) indicates that the calculated flexural deflection of single-curvature was 167% higher than that of the calculated flexural deflection of double curvature. The reason is that flexural stiffness of single-curvature is much smaller than flexural stiffness of double-curvature. Therefore, deformation is larger for single-curvature bending than that of double-curvature bending. In the case of single-curvature bending, the dominant failure mode is flexure. Due to this failure mode, the shear force of single-curvature wall can not reach its maximum value, and its shear deflection contribution is therefore lower than that of the double-curvature wall. As demonstrated in Fig. 13(c), the shear deflection of single-curvature wall is 23% less than that of the double-curvature wall. Due to the curvature bending, the slip deflection contribution of the single-curvature wall was 38% higher than that of the double-curvature wall. The above comparison of single and double curvatures reveals that the shift from double-curvature to single-curvature increases the contribution of flexural deflection, and decreases the contribution of shear deflection. In wall specimens with height to length ratio close to 2, double-curvature bending can enhance the strength and reduce the deflection of the wall as compared to the single-curvature bending values.

6. Conclusions

This study presents a model of ultimate strength and corresponding deflection prediction of reinforced concrete squat walls subjected to double-curvature bending. A comparison of the proposed model with some available test results reported in the literature gives the following conclusions:

1. The ultimate strength with shear failure mode of squat walls can be predicted reasonably well using the softened strut-and-tie model.
2. The corresponding lateral deflection of walls can be estimated with reasonable accuracy by superposition of its flexibility sources of shear, flexure and slip.
3. The calculated results of the proposed procedure correlate reasonably well with the experimental results in terms of the prediction of failure mode, the ultimate strength and its corresponding deflection. Strain predictions of shear reinforcement correlate well with the tendency of the measured strains but don't agree well with the values of measured strains.
4. Shear deflection dominates the contribution of the total deflection of double-curvature walls with height to length ratio not exceeding 2. In this study, the calculated flexural deflection of specimens with H_n/ℓ_w = 2.0 can reach 22% of the total deflection, and the specimens with H_n/ℓ_w = 0.7 can only reach 2%.

Acknowledgements

The authors are grateful to Church Development Service - An Association of the Protestant Churches in Germany (EED) for the scholarship that made this study possible. The authors also gratefully acknowledge the funding supports of the National Center for Research on Earthquake Engineering of the Republic of China and the National Taiwan University of Science and Technology, as well as the valuable contributions of Prof. Yaw-Shen Tu of De Lin Institute of Technology, Taipei, Taiwan, Republic of China.

References

American Concrete Institute (ACI) Committee 318 (2005), *Building Code Requirements for Structural Concrete*, ACI 318-05, Farmington Hills, Michigan.

Comité Euro-Internation du Beton (CEB)-Fédération International de La Precontrainte (FIP) (1993), *Model Code 1990, 1993, (MC90)*, Thomas Telford, London.

Fintel, M. (1991), "Shearwalls – An answer for seismic resistance?", *Concrete Int.*, ACI, **13**(7), 48-53.

Foster, S.J. and Gilbert, R.I. (1996), "The design of nonflexural members with normal and high-strength concretes", *ACI Struct. J.*, **93**(1), 3-10.

Hidalgo, P.A., Ledezma, C.A. and Jordan, R.M. (2002), "Seismic behavior of squat reinforced concrete shear walls", *Earthq. Spectra*, **18**(2), 287-308.

Hsu, T.T.C. (1993), *Unified Theory of Reinforced Concrete,* CRC Press, Inc., Boca Raton, Florida, 313pp.

Hwang, S.J. and Lee, H.J. (1999), "Analytical model for predicting shear strengths of exterior reinforced concrete beam-column joints for seismic resistance", *ACI Struct. J.*, **96**(5), 846-857.

Hwang, S.J., Fang, W.H., Lee, H.J. and Yu, H.W. (2001), "Analytical model for predicting shear strengths of squat walls", *J. Struct. Eng.*, ASCE, **127**(1), 43-50.

Hwang, S.J. and Lee, H.J. (2002), "Strength prediction for discontinuity regions by softened strut-and-tie model", *J. Struct. Eng.*, ASCE, **128**(12), 1519-1526.

Lopes, M.M.P.S. (1991), "Seismic behavior of reinforced concrete walls with low shear ratio", *PhD Thesis*, Civil Engineering Department, University of London.

Sezen, H. (2002), "Seismic behavior and modeling of reinforced concrete building columns", *PhD Dissertation*, Department of Civil and Environmental Engineering, University of California, Berkeley.

Sozen, M.A., Monteiro, P., Moehle, J.P. and Tang, H.T. (1992), "Effects of cracking and age on stiffness reinforced concrete walls resisting in-plane shear", *A Proc. of the Fourth Symposium on Nuclear Power Plant Structures, Equipment, and Piping*, North Carolina State University, Raleigh, NC, December, pp. 3.1-3.13.

Tu, Y.S., Hwang, S.J. and Yu, H.W. (2006), "Prediction of load deflection responses of low rise shear walls", *The Eight U.S. National Conference on Earthquake Engineering (8NCEE)*, San Francisco, April.

Vecchio, F.J. (1998), "Lessons from the analysis of a 3-D concrete shear wall", *Struct. Eng. Mech.*, **6**(4), 439-455.

Vecchio, F.J. and Collins, M.P. (1993), "Compression response of cracked reinforced concrete", *J. Struct. Eng.*, ASCE, **119**(12), 3590-3610.

Yu, H.W. and Hwang, S.J. (2005), "Evaluation of softened truss model for strength prediction of reinforced concrete squat walls", *J. Eng. Mech.*, ASCE, **131**(8), 839-846.

Zhang, L.X.B. and Hsu, T.T.C. (1998), "Behavior and analysis of 100 MPa concrete membrane elements", *J. Struct. Eng.,* ASCE, **124**(1), 24-34.

Appendix illustrative example

Calculate the ultimate shear strength and corresponding deflection of specimen SW11 (Lopes 1991) shown schematically in Fig. A.

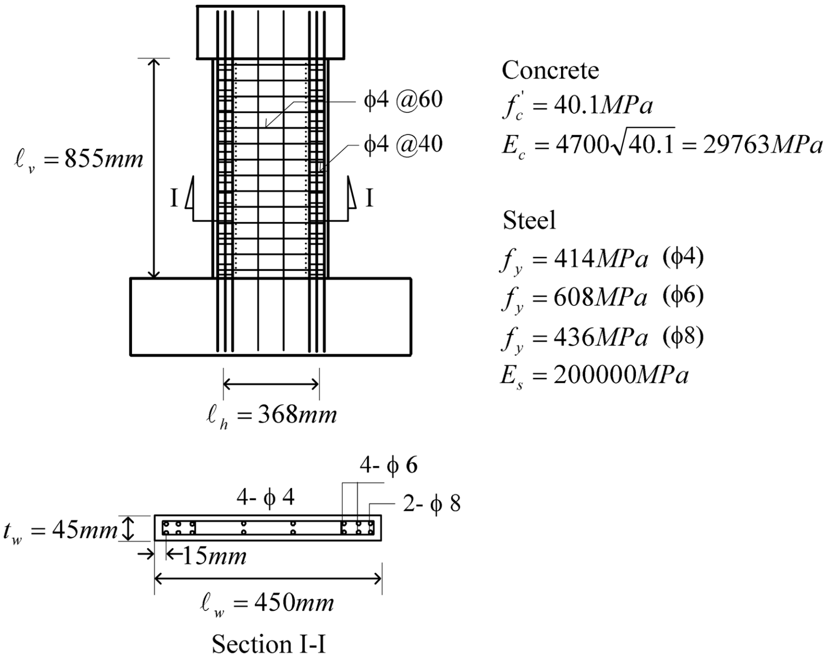

Fig. A Illustrative example of specimen SW11 (Lopes 1991)

Flexural strength

Nominal flexural strength of wall at base equals to 51451 kN-mm according to sectional analysis.

$H_{n,t} = 0.42 \times 855 = 360$ mm

$H_{n,b} = 855 - 360 = 495$ mm

$V_f = 51451/495 = 103.9$ kN

Shear strength

- Properties of softened strut-and-tie model:

$a_w = 123.5$ mm from sectional analysis

$\ell_h = 450 - 2 \times (123.5/3) = 368$ mm

$\theta = \tan^{-1}(\ell_v/\ell_h) = \tan^{-1}(855/368) = 66.73^{\circ}$

$A_{str} = a_w \times t_w = 123.5 \times 45 = 5557$ mm^2

$A_{th} = (2 \times 7 + 0.5 \times 2 \times 7) \times 12.57 = 264$ mm^2 (Hwang and Lee 1999)

$F_{yh} = 264 \times 414/1000 = 109.3$ kN

$A_{th} = 2 \times 2 \times 12.57 = 50.28$ mm^2 (Hwang and Lee 1999)

$F_{yv} = 50.28 \times 414/1000 = 20.8$ kV

$\zeta = 3.35/\sqrt{f_c'} = 3.35/\sqrt{40.1} \le 0.52$; take $\zeta = 0.52$

- Force distribution:

$\gamma_h = (2\tan\theta - 1)/3 = (2\tan 66.73^\circ - 1)/3$; $0 \le \gamma_h \le 1$; take $\gamma_h = 1$

$\gamma_v = (2\cot\theta - 1)/3 = (2\cot 66.73^\circ - 1)/3$; $0 \le \gamma_v \le 1$; take $\gamma_v = 0$

- Balanced amounts of tie forces:

$\overline{K}_h = 1/[1 - 0.2(\gamma_h + \gamma_h^2)] = 1/[1 - 0.2(1 + 1^2)] = 1.667$

$\overline{K}_v = 1/[1 - 0.2(\gamma_v + \gamma_v^2)] = 1/[1 - 0.2(0 + 0^2)] = 1$

$\overline{F}_h = \gamma_h \overline{K}_h \zeta f_c' A_{str} \cos\theta = 1 \times 1.667 \times 0.52 \times 40.1 \times 5557 \times \cos 66.73^\circ/1000 = 76.3$ kN

$\overline{F}_v = \gamma_v \overline{K}_v \zeta f_c' A_{str} \sin\theta = 0$ kN

- Tie index:

$K_h = 1 + (\overline{K}_h - 1) F_{yh}/\overline{F}_h = 1 + (1.667 - 1) \times 109.3/76.3 \le \overline{K}_h$; take $K_h = 1.667$

$K_v = 1 + (\overline{K}_v - 1) F_{yv}/\overline{F}_v = 1 + (1 - 1) \times 20.8/0 \le \overline{K}_v$; take $K_v = 1.0$

- Result:

$V_s = (K_h + K_v - 1)\zeta f_c' A_{str} \cos\theta = (1.667 + 1 - 1) \times 0.52 \times 40.1 \times 5557 \times \cos 66.73^\circ/1000 = 76.3$ kN

Ultimate strength

$V_u =$ smaller of $(103.9, 76.3) = 76.3$ kN

$V_{test}/V_u = 92.6/76.3 = 1.21$

Corresponding deflection

- Shear deflection:

$R_h = \gamma_h(1 - \gamma_v)/(1 - \gamma_h \gamma_v) = 1(1 - 0)/(1 - 0) = 1$

$R_v = \gamma_v(1 - \gamma_h)/(1 - \gamma_h \gamma_v) = 0$

$F_h = R_h V_u = 1 \times 76.3 = 76.3$ kN

$F_v = R_h V_u \tan\theta = 0 \times 76.3 \times \tan 66.73^\circ = 0$ kN

$\varepsilon_h = F_h/(A_{th} E_s) = 76.3 \times 10^3/(264 \times 200000) = 0.00145 \le \varepsilon_y$

$\varepsilon_v = F_v/(A_{tv} E_s) = 0/(50.28 \times 200000) = 0 \le \varepsilon_y$

$\varepsilon_0 = \max[0.002 + 0.001(f_c' - 20)/80, 0.002] = 0.00225$

$-\varepsilon_d = \zeta \varepsilon_0 = 0.52 \times 0.00225 = 0.00117$

$\varepsilon_r = \varepsilon_h + \varepsilon_v - \varepsilon_d = 0.00145 + 0 + 0.00117 = 0.00262$

$\gamma_{vh} = 2(\varepsilon_r - \varepsilon_d)\sin\theta\cos\theta$

$= 2(0.00262 + 0.00117)\sin 66.73^\circ \cos 66.73^\circ = 0.00275$

$\delta_s = \gamma_{vh} \cdot H_n = 0.00275 \times 855 = 2.35$ mm

- Flexural deflection:

$\delta_f = V_u H_n^2 (2H_{n,b} - H_{n,t})/(6E_c I_e)$

$= 76.3 \times 855^2 (2 \times 495 - 360)/(6 \times 29763 \times 0.35 \times 45 \times 450^3/12) = 1.64$ mm

- Slip deflection:

$M_b = 76.3 \times 495 = 37769$ kN-mm when V_u occurs

$f_s = 436$ MPa from sectional analysis

$\theta_{slip,b} = d_b f_s^2/[8uE_s(d_o - a_w)]$

$= 8 \times 436^2/(8 \times \sqrt{40.1} \times 200000 \times [(450 - 15) - 123.5]) = 4.82 \times 10^{-4}$

$M_t = 76.3 \times 360 = 27468$ kN-mm

$f_s = 436 \times 27468/37769 = 317$ MPa

$\theta_{slip,t} = 8 \times 317^2/(8 \times \sqrt{40.1} \times 200000 \times [(450 - 15) - 123.5]) = 2.55 \times 10^{-4}$

$\delta_{slip} = \theta_{slip,t} H_{n,t} + \theta_{slip,b} H_{n,b} = 2.55 \times 10^{-4} \times 360 + 4.82 \times 10^{-4} \times 495 = 0.33$ mm

- Total deflection:

$\delta_u = \delta_s + \delta_f + \delta_{slip} = 2.35 + 1.64 + 0.33 = 4.32$ mm

$\delta_{test}/\delta_u = 4.7/4.32 = 1.09$